JOURNAL OF COMPUTATIONAL PHYSICS **147,** 219–228 (1998)
ARTICLE NO. CP986089

Grid Refinement for Lattice-BGK Models

Olga Filippova and Dieter Hänel

Institute of Combustion and Gasdynamics, University of Duisburg, D-47048 Duisburg, Germany
E-mail: haenel@vug.uni-duisburg.de

Received March 4, 1998; revised August 10, 1998

Lattice–Boltzmann models, proposed at the end of the 1980s as the noise-free version of lattice–gas models, are based on gas-kinetic representation of fluid flow. Their recent modifications, the lattice BGK models, provide especially simple, effective and stable algorithms for the solution of hydrodynamical problems. A local second-order grid refinement scheme for the lattice–BGK model is proposed in this work. The refinement scheme and a boundary-fitting scheme for complicated geometries are applied to simulate a benchmark problem of flow past a cylinder in a channel with small and moderate Reynolds numbers.

Key Words: lattice-BGK model; grid refinement.

1. INTRODUCTION

The lattice–Boltzmann method [1, 2] and its recent modification, the lattice–BGK (LBGK) method [3–6] provide an alternative method for solving continuum problems on a kinetic basis. The computational method is based on the development of discrete molecular velocity distribution functions on uniform Cartesian lattices with additional diagonal links. Hydrodynamic variables are computed at the nodes as moments of the discrete distribution function. The resulting algorithm has been shown to be simple and efficient for computations of incompressible, viscous flows over complex boundaries.

An essential advantage of the LBGK method is the ease and accuracy in dealing with complicated boundary geometries. In the range of small to moderate ($O(10^2)$) Reynolds numbers, where the flow solution is not too anisotropic, the lattice–BGK method is competitive or even superior to conventional CFD methods if dealing with flows in complex geometries as in filters [7] or through granular material.

At higher Reynolds numbers the solution becomes strongly anisotropic due to the presence of very thin boundary layers. Then the application of the lattice–BGK method leads to resolution problems for such layers. However, the difficulties are essentially related to the use of Cartesian-like grids, rather than to the lattice–BGK concept.

One way to reduce the difficulties at high Reynolds numbers is the use of body-conform, curvilinear meshes with clustering of grid points in critical zones, a convenient way used

0021-9991/98 $25.00

in conventional CFD methods. A promising approach for extending the LBGK method to curvilinear grids was published recently by He and Doolen [8, 9], based on the interpolation strategy proposed in [10]. Using an additional finer Cartesian-like lattice and corresponding interpolation strategy they were able to compute results at higher Reynolds numbers. This concept is based on the fixed time-step defined by underlying fine LBGK lattice.

A different way to deal with locally anisotropic solutions is the concept of hierarchical grid refinement which we follow in this paper. This concept is widely used in conventional CFD methods, e.g. in the method of adaptive mesh refinement (AMR) proposed by Berger and Colella [11] and Quirk [12] and applied by the authors, e.g. in [13]. The calculation is based on a coarse grid covering the whole integration domain. In a critical region, detected either by adaptation criteria or defined *a priori*, a finer grid is superposed to the basic, coarser grid. The calculation proceeds with large time steps accordingly to the coarse grid while on the finer grids several time-steps are performed to advance to the same time level.

The aim of the present study is to adopt this hierarchical refinement concept to the LBGK method. In contrast to conventional methods the employment of locally refined patches requires more care since the lattice represents the phase space, i.e. the molecular velocity and the local coordinates.

2. BASIC ALGORITHM

The lattice–BGK model is described by the rate of change of a discrete velocity distribution function [5, 6]:

$$f_{pi}(t+\delta_t, \mathbf{r}+\mathbf{c}_{pi}\delta_t) = f_{pi}(t,\mathbf{r}) + \omega\left[f_{pi}^{\mathrm{eq}}(t,\mathbf{r}) - f_{pi}(t,\mathbf{r})\right]. \tag{1}$$

The equilibrium distribution function is a discrete analog of the Maxwellian distribution function [5, 6]. For the simulation of incompressible flows with density $\rho_0 = 1$ one can take it in the form [14, 15],

$$f_{pi}^{\mathrm{eq}} = t_p\left[\frac{p}{c_s^2} + \frac{u_\alpha c_{pi\alpha}}{c_s^2} + \frac{u_\alpha u_\beta}{2c_s^2}\cdot\left(\frac{c_{pi\alpha}c_{pi\beta}}{c_s^2} - \delta_{\alpha\beta}\right)\right], \tag{2}$$

where $c_s = c/\sqrt{3}$, $c = \delta_x/\delta_t$, and δ_x is the lattice spacing. The Knudsen number of the system ϵ is defined as the ratio between lattice spacing δ_x and characteristic length of the system. Using Chapman–Enskog and Taylor expansions in a series of Knudsen number it can be proved [7, 14, 15] that the zero and first moments of lattice–BGK equation Eq. (1) provide the incompressible Navier–Stokes equations with second-order accuracy in space if the Mach number of the flow is in the order of the Knudsen number ϵ and less. The usual boundary conditions on rigid surfaces used in lattice-gas models as, for example, bouncing-back conditions or "equilibrium-state" conditions [16] decrease, however, the accuracy of the solution near curved surfaces to first order [17]. Even improved boundary conditions proposed in [18, 19] did not consider the location of an arbitrary curved boundary between the nodes of the lattice and in applications to arbitrary geometries actually remained at the order lower than the order of the scheme itself.

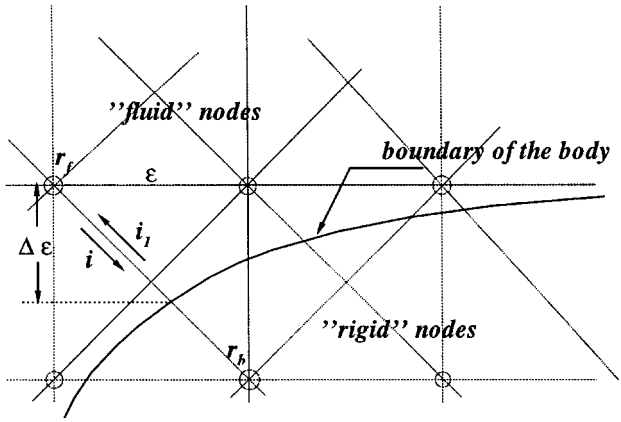

FIG. 1. Computational mesh and geometrical relations for fitting of solid boundaries.

Boundary-fitting conditions proposed earlier by the authors in [7] for steady-state flows enable second-order accuracy at boundaries of arbitrary shape in consistency with the inner scheme.

3. BOUNDARY-FITTING CONCEPT

A curved boundary lying between the nodes of the uniform lattice of a size ϵ is sketched in Fig. 1. If the values of velocity on the boundary $\mathbf{u}^g$ are known ($u^g \equiv 0$ for no-slip conditions, $u^g \neq 0$ for the boundary of porous body) then the distribution function coming to the "fluid" node $\mathbf{r}_f$ from the "rigid" one $\mathbf{r}_b$ is prescribed to be

$$f_{pi_1}(t+\delta_t, \mathbf{r}_f) = \left[(1-\omega) f_{pi}(t, \mathbf{r}_f) + \omega f_{pi}^{\mathrm{eq}}(t, \mathbf{r}_f)\right](1-\omega_i) + a_1\omega_i f_{pi}^{\mathrm{eq}}(t, \mathbf{r}_b) + a_2\omega_i f_{pi}^{\mathrm{eq}}(t, \mathbf{r}_f) - 2t_p \frac{u_\alpha^g c_{pi\alpha}}{c_s^2}, \quad (3)$$

where ω is the relaxation parameter in the "fluid" nodes, $\mathbf{c}_{pi_1} = -\mathbf{c}_{pi}$, $a_1 \cdot a_2 = 0$, and $a_1^2 + a_2^2 = 1$. The "equilibrium distribution function" in the "rigid" nodes $f_{pi}^{\mathrm{eq}}(t, \mathbf{r}_b)$ is defined as

$$f_{pi}^{\mathrm{eq}}(t, \mathbf{r}_b) = t_p\left(\frac{p(t, \mathbf{r}_f)}{c_s^2} + \frac{u_\alpha(t, \mathbf{r}_b)c_{pi\alpha}}{c_s^2} + \frac{u_\alpha(t, \mathbf{r}_f)u_\beta(t, \mathbf{r}_f)}{2c_s^2}\left(\frac{c_{pi\alpha}c_{pi\beta}}{c_s^2} - \delta_{\alpha\beta}\right)\right), \quad (4)$$

where ω_i is the adjusting parameter, $\mathbf{u}(t, \mathbf{r}_b)$ is the linear extrapolated value of $\mathbf{u}$ from the node $\mathbf{r}_f$ through the known value on the boundary:

$$\mathbf{u}(t, \mathbf{r}_b) = \frac{\Delta - 1}{\Delta}\mathbf{u}(t, \mathbf{r}_f) + \frac{\mathbf{u}^g}{\Delta}.$$

The projection of velocity $u_\alpha^g c_{pi\alpha}$ is taken in the crossing point of the boundary and link i.

Taking into account that $\nabla p \sim O(M^2)$ and considering flows with characteristical times $\sim (M\epsilon)^{-1}$, one can estimate the first term in Chapman–Enskog expansion as

$$f_{pi}^{(1)}(t, \mathbf{r}) = -\frac{1}{\omega}\frac{\partial f_{pi}^{\mathrm{eq}}(t, \mathbf{r})}{\partial x_\alpha}c_{pi\alpha} + O(M^2) = -\frac{t_p}{\omega c_s^2}\frac{\partial u_\beta}{\partial x_\alpha}c_{pi\alpha}c_{pi\beta} + O(M^2). \quad (5)$$

Then one can obtain from Eqs. (3)–(5)

$$
\begin{aligned}
&f_{pi_1}(t+\delta_t, \mathbf{r}_f) \\
&\quad = f^{\mathrm{eq}}_{pi_1}(t, \mathbf{r}_f) + \epsilon f^{(1)}_{pi_1}(t, \mathbf{r}_f) + O(M\epsilon^2) \\
&\quad = f^{\mathrm{eq}}_{pi}(t, \mathbf{r}_f) - 2t_p \frac{u_\alpha(t, \mathbf{r}_f) c_{pi\alpha}}{c_s^2} + \epsilon f^{(1)}_{pi}(t, \mathbf{r}_f) + O(M\epsilon^2) \\
&\quad = (1-\omega_i)\big(f^{\mathrm{eq}}_{pi}(t, \mathbf{r}_f) + \epsilon f^{(1)}_{pi}(t, \mathbf{r}_f)(1-\omega)\big) \\
&\qquad + a_1 \omega_i t_p \left(\frac{p(t, \mathbf{r}_f)}{c_s^2} + \frac{u_\alpha(t, \mathbf{r}_b) c_{pi\alpha}}{c_s^2} + \frac{u_\alpha(t, \mathbf{r}_f) u_\beta(t, \mathbf{r}_f)}{2c_s^2} \left(\frac{c_{pi\alpha} c_{pi\beta}}{c_s^2} - \delta_{\alpha\beta} \right) \right) \\
&\qquad + a_2 \omega_i t_p \left(\frac{p(t, \mathbf{r}_f)}{c_s^2} + \frac{u_\alpha(t, \mathbf{r}_f) c_{pi\alpha}}{c_s^2} + \frac{u_\alpha(t, \mathbf{r}_f) u_\beta(t, \mathbf{r}_f)}{2c_s^2} \left(\frac{c_{pi\alpha} c_{pi\beta}}{c_s^2} - \delta_{\alpha\beta} \right) \right) \\
&\qquad - 2t_p \frac{u^g_\alpha c_{pi\alpha}}{c_s^2}.
\end{aligned} \tag{6}
$$

Taylor expansion in a series of Knudsen number ϵ provides

$$
\mathbf{u}(t, \mathbf{r}_f) - \mathbf{u}^g = -\partial_\alpha \mathbf{u}(t, \mathbf{r}_f) \Delta \epsilon c_{pi\alpha} + O(M\epsilon^2).
$$

Equating the coefficient of the first-order term in Eq. (6) to zero, one can obtain the relationship between ω_i and Δ,

$$
\omega_i = \omega(2\Delta - 1), \quad a_1 = 1, \quad a_2 = 0;
$$

$$
\omega_i = \omega \frac{(2\Delta - 1)}{(1-\omega)}, \quad a_1 = 0, \quad a_2 = 1,
$$

where ω is the relaxation parameter in the "fluid" nodes. The remaining terms in Eq. (6) are in the order of $M\epsilon^2$, $M^2\epsilon$ and for flows with $M \sim \epsilon$ can be included in the first-order term in the Taylor expansion of velocity in the "fluid" node $\mathbf{r}_f$ which now can be written as

$$
\mathbf{u}(t, \mathbf{r}_f) - \mathbf{u}^g = -\partial_\alpha \mathbf{u}(t, \mathbf{r}_f)(\Delta + a\epsilon)\epsilon c_{pi\alpha}, \quad a = O(1).
$$

This means that the position of the boundary in the space is defined with accuracy $\sim\epsilon^2$ that is one order higher than in the case of bouncing-back or "equilibrium state" conditions.

The boundary-fitting conditions (Eq. (3)) are introduced into the usual lattice–Boltzmann "stream-and-collide" procedure. They provide the solution of incompressible flow with second-order accuracy for flows with characteristical times $\sim(M\epsilon)^{-1}$ (this accuracy is consistent to the exterior LBGK scheme). For reasons of stability the following combination of boundary-fitting conditions has to be used in Eq. (3):

$$
\omega_i = \omega(2\Delta - 1), \quad a_1 = 1, \quad a_2 = 0, \quad \Delta \geq 0.5,
$$

$$
\omega_i = \omega \frac{(2\Delta - 1)}{(1-\omega)}, \quad a_1 = 0, \quad a_2 = 1, \quad \Delta < 0.5.
$$

4. LOCAL GRID REFINEMENT

Local grid refinement is applied to regions where large changes of solution are expected. The use of locally refined patches superposed to the global coarse grid saves, in general, memory and computational time and enables a high resolution where needed. Grid refinement is performed by dividing the space step through a refinement factor n. The kinematic viscosity, defined in the frame of the LBGK model, depends on the step size with $\nu = (2/\omega - 1)\delta_x c/6$. To achieve the same viscosity and, thus, the same Reynolds number on coarse grids (δ_x^c) and fine grids ($\delta_x^f = \delta_x^c/n$), the relaxation parameter ω in Eq. (1) has to be redefined [20] by

$$\omega_f = \frac{2}{1 + n(2/\omega_c - 1)}. \tag{7}$$

Here ω_f and ω_c are the relaxation parameters on the fine and coarse grids, respectively. Remaining in the over relaxation region ($\omega_f > 1$) and taking into account that when ω_c is too close to 2 the LBGK scheme becomes unstable, one can estimate from Eq. (7) the upper limit of the parameter of refinement n. It depends on the specific problem; usually the upper limit of n is about 50.

The time-step on the fine grid is correspondingly reduced by $\delta_t^f = \delta_t^c/n$, where δ_t^c is the time-step on the coarse grid. The second term in the Chapman–Enskog expansion,

$$f_{pi} = f_{pi}^{\mathrm{eq}} + \epsilon f_{pi}^{(1)} + \epsilon^2 f_{pi}^{(2)} + \cdots \tag{8}$$

for the lattice–BGK model, Eq. (1), depends on the relaxation parameter ω:

$$f_{pi}^{(1)} = -\frac{1}{\omega}\left(\frac{\partial f_{pi}^{\mathrm{eq}}}{\partial t} + \frac{\partial f_{pi}^{\mathrm{eq}}}{\partial x_\alpha} c_{pi\alpha}\right). \tag{9}$$

Since ω changes with the grid size and because the hydrodynamical variables and their derivatives have to be continuous over the interface between two grids, one can obtain from Eqs. (1), (2), (7), (8), and (9) the following relationships between postcollision distribution functions out-coming from the nodes of the coarse and fine grids, respectively:

$$f_{pi}^{\mathrm{post,coarse}} = f_{pi}^{\mathrm{eq,fine}} + \left(f_{pi}^{\mathrm{post,fine}} - f_{pi}^{\mathrm{eq,fine}}\right) \cdot \frac{(1-\omega_c)\omega_f n}{\omega_c(1-\omega_f)} \tag{10}$$

$$f_{pi}^{\mathrm{post,fine}} = \tilde{f}_{pi}^{\mathrm{eq,coarse}} + \left(\tilde{f}_{pi}^{\mathrm{post,coarse}} - \tilde{f}_{pi}^{\mathrm{eq,coarse}}\right) \cdot \frac{\omega_c(1-\omega_f)}{(1-\omega_c)\omega_f n}. \tag{11}$$

Here the values $\tilde{f}_{pi}$ define the spatially and temporally interpolated values of the distribution function from the coarse grid.

The numerical realization is the following. The whole computational domain is covered with the coarse grid. Patches of fine grids are defined in certain regions, e.g. around a solid body. Values of the distribution functions on the coarse grid which are coming from regions of finer patches, including high gradients of hydrodynamical variables, are calculated in the nodes common to both grids, according to Eq. (10). At the time $t = t_0 + \delta_t^c$ after one "streaming-collision" step on the coarse grid the new values of $f_{pi}^{\mathrm{post,coarse}}(t, \mathbf{r})$ are known on the boundary of the patch. With second-order interpolation in space and time one can calculate the values of $f_{pi}^{\mathrm{post,fine}}$, according to Eq. (11) in the boundary nodes of the fine grid

at the time t_0, $t_0+\delta_t^f, \ldots, t_0+\delta_t^f(n-1)$. The calculation proceeds n "streaming-collision" steps on the fine grid.

The parallelization performs well as on uniform grids. For load balance one has to take care for the different regions of refinement and the corresponding different time-steps.

5. TEST CALCULATIONS

Test calculations are performed for 2D benchmark problems of incompressible flows defined in [21] and validated by many computations and partially by experiments. These problems concern steady and unsteady flows around a circular cylinder placed nonsymmetrically in a long rectangular channel. Two typical problems are selected from this benchmark, a steady-state problem at $\mathrm{Re}=20$ and an unsteady problem at $\mathrm{Re}=100$, resulting in a periodical vortex street. The present computations are performed on a coarse grid (221×43 nodes) with a patch of refinement n around the body. The maximum velocity U at the entrance in units of molecular speed c is equal to 0.1 ($U/c\sim\epsilon$).

Results for the steady case at $\mathrm{Re}=20$ with refinement factor $n=4$ ($\omega_c=5/3$) are presented in Table I for some variations of the scheme. The table shows the coefficients for drag and lift, the pressure difference between the front and end points of the cylinder, and the recirculation length. The first row represents results with the present second-order connection on the interfaces between two grids but with first-order boundary conditions (bouncing-back) on the body surface. The second and third rows represent results with boundary-fitting conditions on the body surface but with first-order connection on the interfaces between the two grids either by using equilibrium distribution functions (second row) or by exchanging distribution functions without rescaling (third row). The fourth row represents results with the second-order accuracy in the whole computational domain that means boundary-fitting conditions and rescaling of the distribution functions on the grid interfaces according to Eq. (10) and Eq. (11). These results agree well in the span-width of reference values [21] shown in the fifth and sixth rows. The pressure field obtained on the coarse and fine grids and the streamlines around the cylinder are shown on Fig. 2 for this case. The isobars cross without disturbances the interfaces between two grids.

Computations at $\mathrm{Re}=100$ with the refinement factor 6 ($\omega_c=1.923$) in the same geometry and stationary inflow result in a periodical vortex street. The periodical solution was initiated by computations of first-order accuracy to accelerate the onset of periodical flow. The patch around the body is refined with a factor of $n=6$.

TABLE I
Steady Flow Around a Cylinder at Re = 20

	C_D	C_L	Δp	L_a
LBGK, 1st-order,	5.34	0.011	0.119	0.08
LBGK, 1st-order	5.28	0.014	0.111	0.08
LBGK, 1st-order	4.97	0.013	0.104	0.09
LBGK, 2nd-order	5.52	0.011	0.116	0.08
Band width of	5.57	0.010	0.117	0.08
Ref. values [21]	5.59	0.011	0.118	0.09

Note. Coefficients of drag C_D and lift C_L, pressure difference Δp between the front and end points of cylinder, recirculation length L_a.

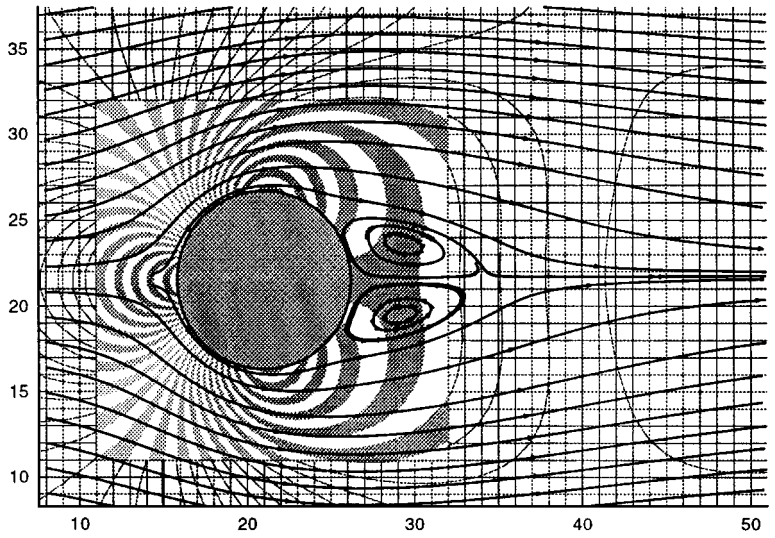

FIG. 2. Steady flow around a cylinder at Re = 20. Presentation of coarse mesh, isobars, and streamlines.

Results of the developed periodical flow are shown in Figs. 3a to 3c for instantaneous isolines of x-velocity in Fig. 3a, for isolines of y-velocity in Fig. 3b, and for isobars in Fig. 3c. Solid lines in Fig. 4 represent drag and lift coefficients and the pressure difference between the front and end points of the cylinder versus the number of coarse time-steps if the second-order accurate boundary-fitting conditions are used. Dashed lines correspond to the same values if the bouncing-back boundary conditions on the surface of the cylinder are used. The dotted straight lines are the upper and lower limits of the amplitudes according

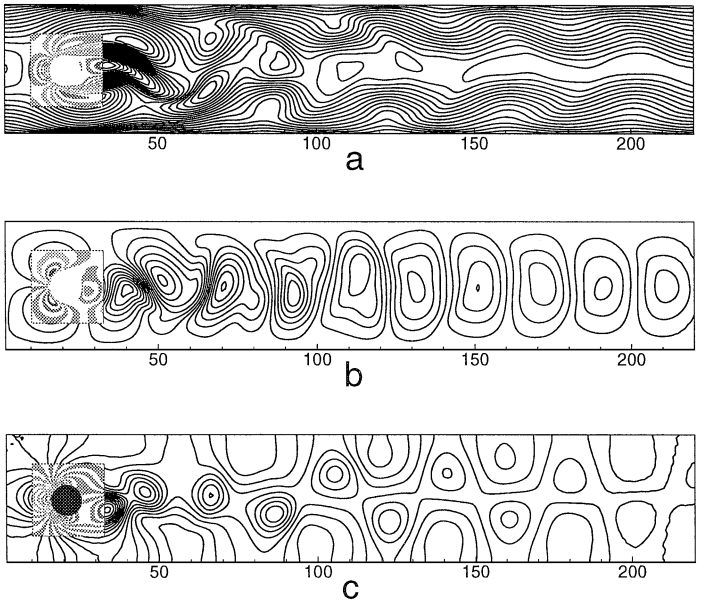

FIG. 3. Unsteady flow around a cylinder at Re = 100: a. instantaneous isolines of x-velocity; b. instantaneous isolines of y-velocity; c. instantaneous isobars.

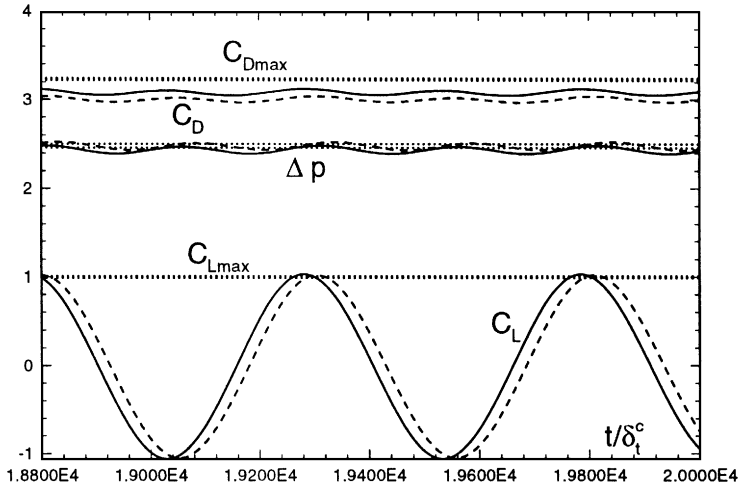

FIG. 4. Unsteady flow around a cylinder at $\mathrm{Re} = 100$. Coefficients of drag C_D and lift C_L and pressure difference Δp between the front and end points of cylinder versus the number of time-steps δ_t^c: solid lines – boundary-fitting conditions; dashed lines – bouncing-back conditions; straight dotted lines – bounds of reference values $C_{D\max}$, $C_{L\max}$, $\Delta p(t_0 + T/2)$ [21].

to the reference values in [21]. They correspond to the maximum drag coefficient, the maximum lift coefficient, and the pressure difference on the cylinder after half-period $T/2$ from the time corresponding to the flow state with the maximum lift coefficient ($t = t_0$). The corresponding time is marked with the hollow circles on the curves $\Delta p(t/\delta_t^c)$ represented in enlarged form in Fig. 5.

The computed Strouhal numbers of 0.297 for the case of bouncing-back and 0.298 for the case of boundary-fitting conditions fit well in the bandwidth 0.295–0.305 of reference values [21]. Like the steady state results, the results obtained with second-order boundary-fitting

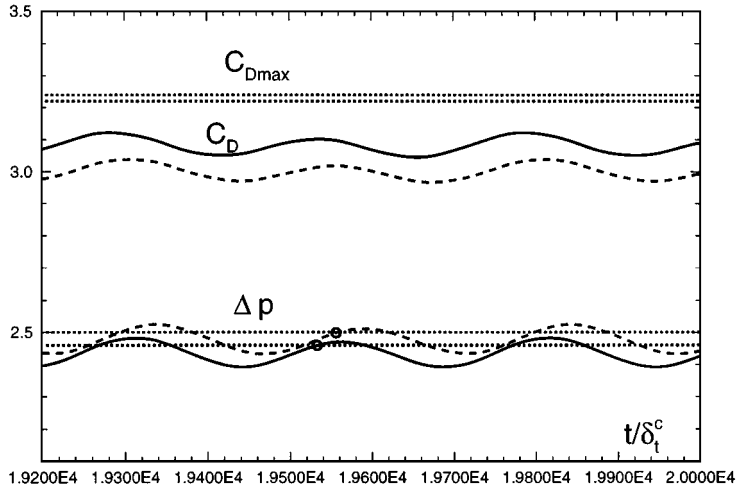

FIG. 5. Unsteady flow around a cylinder at $\mathrm{Re} = 100$. Drag coefficient C_D and pressure difference Δp between the front and end points of cylinder versus the number of time-steps δ_t^c: solid lines – boundary-fitting conditions; dashed lines – bouncing-back conditions; straight dotted lines – bounds of reference values $C_{D\max}$, $\Delta p(t_0 + T/2)$ [21]. (Enlarged upper part of Fig. 4.)

conditions for unsteady problems agree well with the reference values [21]. Notice that the results obtained with bouncing-back boundary conditions are also in good agreement with the reference values [21]. It is connected with the fact that in calculations of lift and drag coefficients hydrodynamical variables as pressure and velocity gradients on the surface of cylinder were calculated by extrapolation of the corresponding values from the flow along the external normal of the cylinder, and the influence of disturbances on the curvilinear surfaces in viscous flow is "smoothed" some distance from it.

The CPU time per cycle on a PA-7200 workstation is 1140 s. It is comparable to the best CPU times of conventional incompressible Navier–Stokes solvers published in [21]; only some multigrid solvers perform faster.

5. CONCLUSIONS

Consequent formulation of the lattice–BGK method to second-order accuracy results in a reliable, accurate, and efficient algorithm for the simulation of incompressible flows at low to moderate Reynolds numbers around complex geometries. Local grid refinement derived from detailed considerations of the model enables economical use of computer capacities and increases the flexibility to deal with anisotropic flow features and thus to deal with higher Reynolds numbers on Cartesian-like lattices. The combination with an adaptive procedure offers a prospective way to an adaptive mesh refinement concept for lattice–BGK methods.

ACKNOWLEDGMENTS

We are grateful to Dr. L.-S. Luo for helpful conversations. This work has been supported by DFG (German Research Society).

REFERENCES

1. G. McNamara and G. Zanetti, Use of the Boltzmann equation to simulate lattice-gas automata, *Phys. Rev. Lett.* **61**, 2332 (1988).
2. F. Higuera, S. Succi, and R. Benzi, Lattice gas dynamics with enhanced collisions, *Europhys. Lett.* **9**, 345 (1989).
3. S. Chen, H. Chen, D. Martinez, and W. Matthaeus, Lattice Boltzmann model for simulation of magnetohydrodynamics, *Phys. Rev. Lett.* **67**(27), 3776 (1991).
4. H. Chen, S. Chen, and W. Matthaeus, Recovery of the Navier–Stokes equations through a lattice gas Boltzmann equation method, *Phys. Rev. A* **45**(8), R5339 (1992).
5. Y. H. Qian, D. d'Humieres, and P. Lallemand, Lattice BGK models for Navier–Stokes equation, *Europhys. Lett.* **17**(6), 479 (1992).
6. S. Chen, Z. Wang, X. Shan, and G. D. Doolen, Lattice Boltzmann computational fluid dynamics in three dimensions, *J. Stat. Phys.* **68**, 379 (1992).
7. O. Filippova and D. Hänel, Lattice Boltzmann simulation of gas-particle flow in filters, *Comput. Fluids* **26**(7), 697 (1997).
8. X. He and G. Doolen, Lattice Boltzmann method on curvilinear coordinates system: Flow around a circular cylinder, *J. Comput. Phys.* **134**, 306 (1997).
9. X. He and G. Doolen, Lattice Boltzmann method on a curvilinear coordinate system: Vortex shedding behind a circular cylinder, *Phys. Rev. E* **56**(1), 434 (1997).

10. X. He, L.-S. Luo, and M. Dembo, Some progress in Lattice Boltzmann method. Part 1. Nonuniform mesh grids, *J. Comput. Phys.* **129**, 357 (1996).
11. M. J. Berger and P. Collela, Local adaptive mesh refinement for shock hydrodynamics, *J. Comput. Phys.* **82**, 67 (1989).
12. J. J. Quirk, An adaptive grid algorithm for computational shock hydrodynamics, Ph.D. thesis, Cranfield Inst. of Technology, UK, 1991.
13. U. Uphoff, D. Hänel, and P. Roth, Influence of reactive particles on the structure of detonation waves, *Comb. in Sci. Technol.* **110**–**111**, 419 (1995).
14. Q. Zou, S. Hou, S. Chen, and G. Doolen, An improved incompressible lattice Boltzmann model for time-independent flows, *J. Stat. Phys.* **81**, 35 (1995).
15. X. He and L.-S. Luo, Lattice Boltzmann model for the incompressible Navier–Stokes equation, *J. Stat. Phys.* **88**, 927 (1997).
16. D. P. Ziegler, Boundary conditions for lattice Boltzmann simulations, *J. Stat. Phys.* **71**, 1171 (1993).
17. I. Ginzbourg and P. M. Adler, Boundary flow condition analysis for the three-dimensional lattice Boltzmann model, *J. Phys. II France* **4**, 191 (1994).
18. S. Chen, D. Martinez, and R. Mei, On boundary conditions in lattice Boltzmann methods, *Phys. Fluids* **8**(9), 2527 (1996).
19. D. R. Noble, S. Chen, J. G. Georgiadis, and R. O. Buckius, A consistent hydrodynamical boundary conditions for the lattice Boltzmann method, *Phys. Fluids* **7**, 203 (1995).
20. O. Filippova and D. Hänel, Boundary-fitting and grid refinement in Lattice-BGK models, in *Proceedings of 7th International Symposium on CFD* (15–19 September 1997, Bejing, China), *Int. Acad. Publishers*, 192 (1997).
21. M. Schäfer and S. Turek, Benchmark computations of laminar flow around a cylinder, in *Notes in Numerical Fluid Mechanics*, (Vieweg Verlag, Braunschweig, 1996), Vol. 52, p. 547.